



EUMETSAT/ECMWF Fellowship Programme Research Report

67

Quality Assessment and Assimilation of Meteosat-12 FCI AMVs

Francis Warrick
November 2025

Report Research Report
ogramme EUMETSAT/ECM
arch Report Research Report
Programme EUMETSAT/E
esearch Report Research F
ship Programme EUMETSA
ERESearch Report Research
owship Programme EUME
port Research Report Research
Fellowship Programme EU
Report Research Report F
WF Fellowship Programme

search Report Research Report Research Report Research Report Fellowship Programme EUMETSAT/ECMWF Fellowship Program Research Report Research

Series: EUMETSAT/ECMWF Fellowship Programme Research Reports

A full list of ECMWF Publications can be found on our web site under:

http://www.ecmwf.int/en/publications/

Contact: library@ecmwf.int

© Copyright 2025

European Centre for Medium Range Weather Forecasts, Shinfield Park, Reading, RG2 9AX, UK

Literary and scientific copyrights belong to ECMWF and are reserved in all countries. The content of this document is available for use under a Creative Commons Attribution 4.0 International Public License. See the terms at https://creativecommons.org/licenses/by/4.0/.

The information within this publication is given in good faith and considered to be true, but ECMWF accepts no liability for error or omission or for loss or damage arising from its use.



Abstract

Meteosat-12 AMVs are a significant upgrade to EUMETSAT's geostationary AMV product, both in terms of making use of enhanced features of the new Meteosat Third Generation Flexible Combined Imager, as well as benefiting from a completely revised AMV derivation algorithm. The superior spatial and temporal resolution of its imager compared to Meteosat Second Generation gives a vast increase in the number of cloud features that can be tracked. Changes made to EUMETSAT's AMV derivation, including the use of a smaller cloud target box, bring improvements to the data quality as well as an additional boost to data volume. There is a significant NWP forecast improvement from swapping the assimilation of Meteosat-10 AMVs for Meteosat-12 AMVs. Best results were achieved with hourly rather than half-hourly assimilation of the Meteosat-12 AMVs. The new Optimal Cloud Analysis height assignment scheme makes a small contribution to the forecast improvement, but the other derivation changes and increased data volume provide a larger benefit. Adding low level night-time AMVs from the 3.8 μ m channel has a neutral to slightly negative forecast impact. After the Meteosat-12 launch in December 2022, problems with the FCI calibration mechanism delayed the arrival of FCI data. However, the cross-calibration MICMICs approach used for the Meteosat-12 imager performs well for AMV data quality which has been consistently high since the data started being received in November 2024. The improved forecast quality given by assimilation of Meteosat-12 AMVs is an early benefit of the MTG-I programme and demonstrates the importance of developing EUMETSAT's AMV derivation. ECMWF was the first NWP centre to begin operational assimilation of the Meteosat-12 AMVs, beginning in June 2025.

1 From Meteosat Second Generation to Meteosat Third Generation

Meteosat Third Generation is the new generation of EUMETSAT's geostationary satellite, and consists of two parallel programmes: MTG-Imager and MTG-Sounder. The first MTG-Sounder launched in July 2025, on board is the first infrared sounder to view Europe and Africa from geostationary orbit. MTG-Imager 1, renamed Meteosat-12 after launch, went into orbit in December 2022 and carries EUMETSAT's first lightning imager, as well as a new infrared and visible imager, the Flexible Combined Imager (FCI). FCI, whose Atmospheric Motion Vector (AMV) wind product is the focus of this report, represents an upgrade on Meteosat Second Generation (MSG)'s Spinning Enhanced Visible and Infrared Imager. A key difference is that FCI spends most of its viewing time looking at Earth thanks to Meteosat-12's three-axis stabilisation, whereas MSG's spin-stabilised design means SEVIRI time spends much of its time looking at deep space. This feature helps FCI to record more information than SEVIRI and offer upgrades in spatial and temporal resolution. Full-disc imagery is now available every 10 rather than 15 minutes, and the resolution of the thermal channels has improved from 3km to 2km, and the narrow-band visible channels have improved from 3km to 1km ¹. FCI is also an upgrade spectrally, with the number of channels increasing from 11 plus one broad-band channel on SEVIRI, to 16 channels on FCI. The specifications of SEVIRI and FCI are given in Table 1.

Both FCI and SEVIRI are designed to calibrate their infrared channels by a combination of looking at deep space and looking at an on-board black body source. However, In January 2024 FCI's on-board calibration mechanism suffered a fault and is no longer available. Instead, a system called MICMICS ² calibrates FCI using external information from co-located Infrared Atmospheric Sounding Interferometer (IASI) onboard EUMETSAT's polar orbiting Metop-B/C satellites. The calibration is then validated by

¹SEVIRI also had a broad-band 'High-Resolution Visible' channel with resolution 1km

²Mission Integrated Calibration Monitoring and Inter-Calibration System



Imager	Spinning Enhanced Visible Infra-Red Imager	Flexible Combined Imager
		444 nm
		510 nm
	High-Resolution Visible	640 nm
	0.635 μm	865 nm
Channels	0.81 μm	914 nm
	1.64 μm	1380 nm
	3.92 μm	1610 nm
	6.25 μm	2250 nm
	7.35 μm	3.80 µm
	8.70 μm	6.30 µm
	9.66 μm	7.35 µm
	10.8 μm	8.70 μm
	12.0 μm	9.66 µm
	13.4 μm	10.50 μm
		12.30 μm
		13.30 μm
Imaging Frequency	Full-Disc: 15 minutes	Full-Disc: 10 minutes
Pixel Size	3km (High-Resolution Visible 1km)	Thermal 2km, Visible 1km.

Table 1: Comparison of SEVIRI and FCI imager channels, **bold** indicates channels used by EUMETSAT for AMV derivation.

CrIS ³ measurements from on-board the NOAA-20/21 satellites which shows that the external calibration is performing well as a replacement for the on-board blackbody source [4].

2 Upgraded EUMETSAT AMV Derivation for MTG

Alongside the improvements to spatial resolution and temporal frequency of full disc images that FCI offers over SEVIRI, there are substantial changes to EUMETSAT's AMV processing between the two generations of satellites which are summarised in Table 2.

In MSG AMV derivation, a cloud feature would be tracked through a sequence of 4 images, giving 3 subvectors between the images, which were then averaged together to give the final AMV. For FCI, only two images are used, with the AMV time set to the second image and no subvector averaging applied. The combination of a change from using 4 images to 2 images for tracking features as well as the change in time separation between full disc images, mean the observing time has changed from 60 minutes to 10 minutes. However a second image pair is used to do the consistency check for the MTG AMV Quality Indicator (QI), so the observing time could be considered to be 20 minutes; MSG uses all 4 subvectors for the consistency check. The MTG AMV product is available half-hourly while MSG AMVs are an hourly product.

The combination of the pixel spatial resolution change and the change in the size of the tracked target from 24 to 16 pixels means the size of a target has reduced from 72km to 32km for the thermal channels and from 72km to 16km for the narrow-band visible channels. The choice of target size is a compromise between too small a target leading to ambiguous matching in the tracking step, and too

³Cross-track Infrared Sounder



large a target averaging separate cloud motions together. The reduction in size of the target in pixels brings the EUMETSAT AMV derivation in line with the recommendation of the International Winds Working Group [3] and other studies [5]. The reduction in target size is also expected by the literature to increase average and maximum AMV wind speeds [7], as well as contributing to the increase in FCI AMV observation count by increasing the number of trackable features, compared to SEVIRI. Figure 1 shows an example of the difference in target sizes, illustrating the effect of the smaller segment size. In the SEVIRI case it can be seen that the target box includes two groups of clouds, one in the centre and one at the bottom. Meanwhile the FCI target box, centred on the same point, contains only the centre group of clouds from the SEVIRI image. In this case the SEVIRI AMV will be the average motion of the two groups of clouds, while the FCI AMV isolates the centre cloud group motion, a situation that is more likely due to the smaller segment size.

Another major change to the AMV derivation is the height assignment scheme. The MSG height assignment scheme, 'Cloud Analysis' (CLA) is based on matching the observed brightness temperature to those simulated by a forecast model. This is done using a scene-dependent approach that usually uses the $10.8~\mu m$ window channel, but can also make use of SEVIRI's other channels in the case of semi-transparent clouds by using the CO2 slicing or water vapour intercept methods [1]. The height assignment method for MTG, Optimal Cloud Analysis (OCA), derives cloud properties using an optimal estimation approach which minimises a cost function to fit the observed brightness temperatures of all the imager channels to their simulated equivalents. A high value from the cost function is known to be an indicator of a multi-layer cloud situation; in these cases OCA will repeat the minimisation to fit a two-layer cloud model. This should alleviate a common problem with AMV height assignment where a semi-transparent upper layer is assigned to the mid-troposphere due to some of the radiation passing through the cloud from a lower, warmer layer, causing a large positive speed bias.

The channels used for AMV derivation are slightly different between the two generations of satellites. For SEVIRI, AMVs were available from the broad-band High Resolution Visible channel which had 1km resolution. Such a channel is not on FCI as the narrow-band visible channels now have 1km rather than 3km resolution. FCI AMVs are available from the 3.8 μ m channel; a similar channel was available on SEVIRI but not used for AMV derivation. This channel, like the visible channels, is useful for identifying low level clouds which are harder to detect in the 10.5 μ m channel due to low temperature difference between the low clouds and the Earth's surface. At the 3.8 μ m wavelength, FCI receives both radiation from Earth's thermal emission and reflected sunlight. The night time imagery can be used to track low level cloud features, providing complementary low level AMV coverage to the daytime visible AMVs. Different infrared emission characteristics between the 10.5 μ m and 3.8 μ m channels means that the 3.8 μ m can be used to reveal the presence of low, warm clouds that the 10.5 μ m channel may miss. The central wavelengths of the other channels used for AMV derivation have changed slightly, for example the infrared window channel is now centred at 10.5 μ m instead of 10.8, while bandwidths have reduced. These changes are not expected to significantly affect the AMV product.

3 Quality Comparison: MTG AMVs Versus MSG AMVs

Background departures are often used to assess AMV quality, because the background (short-range forecast) from an NWP system provides a stable reference for comparisons, benefitting from a wealth of observations in previous assimilation windows that is carried forward in time through the forecast model. Another advantage of background departures over measuring AMV quality against other wind observations is that the background is unbiased spatially, whereas the conventional wind observations are clustered around busy flight paths and densely populated areas. The background departures used in



Parameter	MSG	MTG
Number of Images in Sequence	4	2 (3 including QI)
Target Box Size	24 pixels	16 pixels
Height Assignment Method	Cloud Analysis (CLA)	Optimal Cloud Analysis
		(OCA)
	Infrared Window 10.8	Infrared Window 10.5
	Water Vapour 6.3	Water Vapour 6.3
Channels Used (µm)	Water Vapour 7.3	Water Vapour 7.3
	Visible 0.8	Visible 0.8
	High-Resolution Visible	Infrared 3.8

Table 2: Comparison of MSG and MTG AMV Derivations

this section were calculated by running an IFS experiment, version CY49R1, resolution TCo399 with forecast length limited to 12 hours. Neither the Meteosat-10 nor Meteosat-12 AMVs were assimilated in the experiment, so as not to unfairly make the background more closely resemble one dataset than the other. The rest of the conventional and satellite observing system, including other AMVs, was assimilated as usual.

In general the data shown in this section are filtered to those with a QI value of at least 85 and those passing a background check against the ECMWF model background which removes AMVs with very large background departures. The QI>85 threshold used in this study is chosen for consistency with ECMWF's operational usage of MSG AMVs which applies the same threshold. We can see from Figure 2 that the QI remains a useful way of removing poorer quality data as shown by the reduction of root-mean-square vector differences (RMSVD) against the background. QI filtering achieves this RMSVD reduction without simply removing the fastest AMVs, indeed the mean AMV speed increases with QI. One curious feature of the QI distribution is that the Meteosat-12 RMSVD increases at the very highest QI values (>95) where there are a high proportion of Meteosat-12 AMVs.

The stability over time and overall similarity in background departures of Meteosat-10 and -12 infrared window AMVs can be seen in Figure 3. The first panel of this Figure shows the vast increase in data volume that results from the combination of spatial and temporal resolution changes. Some reductions in Meteosat-12 data volume can be seen on occasional days, these are a result of processing problems. There are also some gaps in the Meteosat-12 AMV production which are related to the commissioning activities of Meteosat-12 and/or the FCI instrument.

The mean and root-mean-square (RMS) background departures are both similar, though the mean background departure is closer to zero for Meteosat-12, and RMS vector difference is slightly higher. Meteosat-12 likely has higher RMSVD values due to its higher mean AMV speeds, causing larger O-B differences in some cases, though not necessarily when normalised by speed. The distribution of RMSVD compared to QI (Figure 2) may also be a reason for the RMSVD of Meteosat-12 being higher than Meteosat-10 when looking only at AMVs with QI > 85, as there are a large number of Meteosat-12 AMVs with QIs near 100 at which point Meteosat-12 RMSVD ticks up above Meteosat-10. The fourth panel shows that the mean speed of Meteosat-12 AMVs is higher, a result in line with predictions from the literature for a reduced target size.

From Figure 4 we can see that for the 6.3 μ m water vapour channel the mean background departure increases from around 0 m/s to around +0.5 m/s. Again, this may be the result of the result of the overall higher mean speed of FCI compared to SEVIRI. Unlike the infrared window channel, here we see no increase in the RMS vector difference despite the higher average wind speed. Similar results were seen



for the water vapour 7.3 μ m channel.

The profiles in Figures 5 and 6 show that the background departures for equivalent FCI/SEVIRI channels are broadly similar. As with the time-series statistics we see higher mean speeds for Meteosat-12 than Meteosat-10, and here we see that this is true for all channels. Furthermore, while the time-series statistics showed Meteosat-12 has a higher mean speed and RMSVD averaged over all vertical levels, here we see this is still the case when we look at different vertical layers of AMVs separately. RMS vector differences are slightly larger for Meteosat-12 than Meteosat-10 in the infrared and visible profiles, or very similar for the two water vapour channels. O-B speed biases are a little higher for Meteosat-12, bringing them closer to 0 m/s for the infrared window channel, but slightly more positive for the $6.3~\mu m$ channel.

From Figure 6 we can see that background departures of the new 3.8 μ m channel are similar to those of the visible channel AMVs. We can also see that above the 700 hPa lid that existed for SEVIRI AMVs, the quality of the upper level visible AMVs is similar to infrared 10.5 μ m AMVs. The background departures for the 3.8 μ m AMVs make them suitable for assimilation. Similarly, the 700 hPa minimum pressure applied in ECMWF data selection for assimilation could be revisited in a future study based on these results.

Figures 7, 8 and 9 show the geographic distribution of the background departures we saw in the profile plots. We see a common pattern in the mean O-B statistics, that negative mean O-Bs present for Meteosat-10 AMVs in the extratropics are greatly reduced for Meteosat-12. This could be a consequence of the change in height assignment method to OCA, as has been seen previously with OCA heights for MSG AMVs [8]. The overall increase in AMV wind speeds with FCI could also contribute to this reduction in mean background departures. In the tropics, a positive mean background departure emerges in the $6.3~\mu m$ channel. Although the positive mean O-B that emerges for the $6.3~\mu m$ channel is quite small at around 1 m/s, the fact that it is so widespread is concerning and a future experiment could test whether there is still a benefit to forecast quality from assimilating this channel in addition to the $7.3~\mu m$ AMVs.

We also see that RMS vector differences and the geographic distribution of AMVs (noting the different scales for MSG and MTG) are largely the same for the two generations of satellite. One small exception is the North Atlantic where MTG records a higher proportion of its AMVs than MSG in the two water vapour absorption channels. The reason for this is not clear, if it was due to the finer spatial resolution of FCI capturing smaller clouds than SEVIRI then we would expect to see the same result in the infrared window channel.

From Figure 10 we can see that where observation density is highest at around 200-400 hPa, mean background departures are reduced in Meteosat-12 AMVs compared to Meteosat-10. This could be a result of the new OCA height assignment, or could be a result of the spatially and temporally finer tracking employed by the Meteosat-12 AMV derivation. The zonal plot also highlights that the stripiness commonly found for low-level Meteosat-10 AMVs both in data counts and bias characteristics is not present for Meteosat-12. The stripiness arises from assigning AMVs to fixed pressure levels in temperature inversion regions after the height assignment step, many more fixed levels are available for in the MTG AMV processing compared to MSG processing.



4 Impact of MTG AMV Assimilation on Forecast Performance

A series of assimilation experiments using ECMWF's IFS model, version CY49R1 were run, in order to test both the overall forecast impact of assimilating Meteosat-12 AMVs and the contribution to this impact from the changes to the imager and AMV derivation compared to MSG. The experiments were run at TCo399 resolution, roughly corresponding to 28km resolution, with the data assimilation system using a final inner loop resolution of around 80km. The study period was from November 2024 to Spring 2025. Data selection of the AMVs was kept the same for MTG and MSG AMVs. This includes a QI threshold of 85, background check to remove AMVs with gross error, and spatial rejections such as of water vapour AMVs below 250 hPa in the tropics, or of any Meteosat AMVs below 500 hPa over land. At ECMWF, AMV observation error estimation combines fixed tracking error profiles with a situation-dependent term that accounts for the AMV's estimated pressure error and the local model wind shear [6]. Tracking and pressure error estimates for the Meteosat-12 AMVs were derived and found to be similar to those used for MSG AMVs, consequently the same errors are used for Meteosat-12. Spatial thinning is also applied using 200km by 200km boxes. Other observations, both satellites that may overlap the Meteosat-10/12 viewing area.

4.1 Overall Assimilation Impact of Meteosat-12 AMVs

In Figure 11, forecast performance is measured by the standard deviation of short range (up to 12 hour) forecasts from a set of observations, in this case conventional wind observations, at the forecast validity time. This style of forecast verification is used repeatedly in this Section.

Firstly, we consider the overall impact of the Meteosat-12 AMVs compared to assimilating the Meteosat-10 AMVs and to not assimilating any AMVs from a 0° longitude geostationary satellite. Figure 11 shows the impact of Meteosat-12 AMVs as measured by forecast fit to conventional winds over the 0° Meteosat disc. Figure 12 shows that Meteosat-12 AMV assimilation further improves the 12-hour forecast agreement with scatterometer winds, beyond the improvement already given by Meteosat-10 AMVs. These results are a significant improvement from adding Meteosat-12 AMVs, a clearly significant improvement over the baseline no-Meteosat experiment. The forecast improvement measured by 12-hour forecast fit to ATMS humidity sensitive channels and geostationary radiances remains the same for Meteosat-12 as it was for Meteosat-10, compared to the no 0° Meteosat reference (not shown).

Figures 13 and 14 show the effect of assimilating Meteosat-10 and Meteosat-12 AMVs on forecast field verification scores, verified against operational ECMWF analyses. In the wind field we see a similar impact although Meteosat-12 assimilation delivers a better wind forecast in the southern hemisphere in the 48 and 120 hour forecasts. In the geopotential height forecast verification, the impact of Meteosat-12 is much clearer, giving a substantially stronger impact in the 12 and 24 hour forecast ranges, which remains significant out to 120 hours lead time. The verification is performed against operational ECMWF analyses in which Meteosat-10 AMVs were assimilated, meaning that the verification slightly favours the Meteosat-10 experiment at short ranges. This makes the finding that Meteosat-12 appears to perform better all the more encouraging.

Figure 15 shows the large increase in assimilated observation count from assimilation of Meteosat-12 AMVs compared to Meteosat-10. This increase is despite the same 200km spatial thinning being used for both experiments, so Meteosat-12 AMV assimilation must be filling additional thinning boxes compared



to Meteosat-10 in order to end up with roughly twice the number of Meteosat-12 AMVs assimilated as the number of Meteosat-10 AMVs that were assimilated. The increase in the number of assimilated AMVs is another benefit of Meteosat-12 AMV assimilation as it improves the robustness of the observing system. As well as the large overall increase in data volume with Meteosat-12, some SEVIRI AMV coverage gaps are filled in with FCI AMVs, likely due to resolving and tracking additional, smaller cloud features [2].

4.2 Size of Impact from OCA Height Assignment

The change from situation-based CLA height assignment, to an optimal estimation approach with optional two layer model with OCA, is a substantial change to EUMETSAT AMV derivation. AMV pressures from the OCA scheme are also available as an alternative pressure with MSG AMVs. By running an additional experiment that uses the OCA pressures for Meteosat-10 AMVs instead of the CLA pressures, we can estimate how much of the Meteossat-12 AMV impact comes from the height assignment change.

In Figure 16 we see that the impact of the change in height assignment in isolation for Meteosat-10 is mostly neutral, though there a some small improvements just short of significance. So we can conclude that most of the benefit of MTG AMV assimilation is due to a combination of the changes in tracking time, spatial resolution and target box size, and the greatly increased volume of data that results.

This finding is in contrast to a previous result that using OCA pressures for MSG AMVs gives a significant forecast improvement. However, the earlier result was obtained for a different study period, and also used OCA pressures for Meteosat-9 (Indian Ocean Data Coverage) AMVs in addition to Meteosat-10. The latter aspect might explain a larger impact from the use of the OCA height assignment than seen here with just one satellite.

4.3 Hourly versus Half-Hourly Assimilation

MTG AMVs are the first geostationary AMV product to be available half-hourly - although full disc imagery from geostationary satellites GOES and Himawari is available every 10 minutes, their AMV products are only provided hourly.

From Figure 17 we can see that, compared to the baseline experiment with no Meteosat AMVs assimilated from the 0°degree longitude position, half-hourly assimilation does not significantly improve the 12 hour forecast fit to ATMS observations for the humidity sensitive channels 19-22, while hourly assimilation at minute=00 does deliver a significant improvement. We can also see that the fit of forecasts to conventional wind observations is improved for both hourly and half-hourly assimilation but that the improvement is larger for the hourly assimilation.

It is likely that the superior performance of hourly assimilation is due to difficulties with temporally correlated errors when assimilating FCI AMVs half-hourly. Generally the temporal error correlations arise from the similarity of cloud features from one tracking period to another, and therefore of height assignment errors for those cloud will also be correlated. This correlation should be reduced when the Meteosat-12 AMVs are separated by 60 rather than 30 minutes.

The choice of using hourly data at minute=00 or minute=30 did not have a significant impact on forecast quality (not shown); minute=00 was chosen for the other experiments in this report.



4.4 Adding the IR 3.8 μ m Channel

This channel is useful for detecting low, warm clouds at night, as there is better contrast with the surface at this wavelength compared to the IR 10.5 / 10.8 μ m channel. This means the 3.8 μ m AMVs could fulfil a similar role to the visible channel AMVs. As we have seen, the background departures are similar between the 3.8 μ m, 10.5 μ m and visible channel AMVs and consequently it was decided to run an additional experiment to test the impact of adding the 3.8 μ m AMVs in addition to the other Meteosat-12 AMVs.

The quality control used was the same as for the visible AMVs: QI threshold of 85, only assimilating the data between 700 hPa and the surface, and only assimilating them over sea because over land no geostationary AMVs are assimilated between the surface and 500 hPa. The 3.8 μ m AMVs are not provided during daytime when there is a contribution from reflected sunlight in this channel, so their usage is automatically restricted to night-time without applying any additional quality control.

The impact of adding these additional AMVs was neutral to slightly negative. While standard deviations of background departures for most observation types are not significantly changed, Figure 18 shows an example for the change in agreement of conventional winds with 12-hour forecasts, with a small negative impact at 300 hPa. More concerning is Figure 19, a small but significant negative impact for 3 out of 4 sources of scatterometer winds. Although the degradation is small, the scatterometer winds are at the ocean surface and the 3.8 μ m AMVs were assimilated between the surface and 700 hPa, suggesting a clear link between adding the 3.8 μ m AMVs and a worse short-range ocean surface wind forecast. The impact on medium range forecast verification was mostly neutral (not shown).

At ECMWF, we also do not assimilate AMVs from the equivalent GOES-ABI channel, while some other NWP centres do assimilate those AMVs. Future work at ECMWF will study the 3.8 / 3.9 μ m AMVs in more detail and investigate whether revised data selection can give a forecast improvement from assimilating these AMVs.

5 Summary

We have seen that the quality of Meteosat-12 AMVs, as measured by background departures, is similar to Meteosat-10 AMVs. The MTG mean AMV speeds are higher than MSG, likely due to a combination of smaller pixels and smaller target boxes. The spatial resolution and smaller target box size result in a manyfold increase in observation count, even if only considering the Meteosat-12 AMVs hourly rather than half-hourly. The lack of on-board calibration for the FCI instrument does not result in any significant problems for FCI AMVs, in fact the MICMICS cross-calibration system seems to work very well for AMV derivation.

The forecast benefit from assimilating MTG AMVs was superior to Meteosat-10. This is a very positive finding, as it demonstrates benefits from the combination of enhanced instrument capabilities and AMV processing updates. Given that that the departure statistics for the Meteosat-12 and Meteosat-10 winds are overall quite similar, it is likely that much of the benefit arises from the increase in assimilated AMV count. Better results were achieved by assimilating Meteosat-12 AMVs hourly rather than half-hourly, likely due to neglected temporal error correlations associated with the AMVs. The change of height assignment to OCA only delivers a small part of the improved forecast impact, the majority therefore comes from the resolution upgrade, smaller target box and reduced observing time. The impact of adding the $3.8~\mu m$ AMVs was neutral to slightly negative.



Future research on the Meteosat-12 AMVs could try to achieve a positive impact from the IR 3.8 μ m AMVs using revised quality control. The 3.8 μ m AMVs are not currently assimilated due to the degraded short-range forecast fit to scatterometer winds. As the mid and upper level IR 3.8 μ m and 10.5 μ m AMVs have similar background departures, this could include revisiting the 700 hPa minimum pressure requirement, which could also be reconsidered for the visible AMVs. The data selection of Meteosat-12 AMVs could also be revisited as there are some changes in mean background departures, especially in the upper troposphere, that could mean we see a benefit from relaxing the current spatial rejections on the use of Meteosat AMVs.

ECMWF was the first NWP centre to begin operational assimilation of Meteosat-12 AMVs into the IFS model on 16 June, using the data hourly and applying the same quality control as is used for MSG AMVs.

6 Acknowledgements

This work was funded by the EUMETSAT Fellowship Programme. Many thanks go to Youva Aoun and Régis Borde of EUMETSAT for providing information on the FCI AMVs.

References

- [1] R. Borde and R. Oyama. A direct link between feature tracking and height assignment of operational atmospheric motion vectors. *Proceedings of the 9th International Winds Workshop, Annapolis, Maryland, USA, 14-18 April 2008, 2008.*
- [2] Javier García-Pereda, Nina Håkansson, and Sara Hörnquist. Nwcsaf/high resolution winds amv software for geostationary and polar satellites: Status in 2025. In *EUMETSAT Meteorological Satellite Conference*, *Lyon*, *France*, 2025.
- [3] International Winds Working Group. Recommendations for AMV Configuration (Version 4), May 2025. Action A46.04 in support of HLPP 4.2.2.
- [4] Ali Mousivand, Christoph Straif, Alessandro Burini, Mounir Lekouara, Vincent Debaecker, Tim Hewison, Stephan Stock, and Bojan Bojkov. In-Flight Calibration of Geostationary Meteorological Imagers Using Alternative Methods: MTG-I1 FCI Case Study. *Remote Sensing*, 17(14):2369, 2025.
- [5] Soo Min Oh, Régis Borde, Manuel Carranza, and In-Chul Shin. Development and Intercomparison Study of an Atmospheric Motion Vector Retrieval Algorithm for GEO-KOMPSAT-2A. *Remote Sensing*, 11(17):2054, 2019.
- [6] K. Salonen and N. Bormann. Atmospheric Motion Vector observations in the ECMWF system: third-year report. *EUMETSAT/ECMWF Fellowship Programme Research Report*, No.32, 2013.
- [7] E. H. Sohn and R. Borde. The Impact of Window Size on Atmospheric Motion Vectors. In *Proceedings of the 9th International Winds Workshop (IWW9)*, 2009.
- [8] Francis Warrick. Progress on the use of Atmospheric Motion Vectors at ECMWF. In *EUMETSAT Research Fellowships: Presentations and Reports 2025*, March 2025. Presentation at the EUMETSAT Research Fellowships event, available at https://www.eumetsat.int/media/51891.



List of Figures

1	Red boxes indicate the size of the AMV target	12
2	Variation of RMSVD against the background, mean AMV speed, and AMV count with forecast-independent quality indicator, for Meteosat-10 and -12 infrared 10.5 / 10.8 μ m channel AMVs, 20241104-20250513. Meteosat-12 AMVs with QI < 30 are available but are not shown here.	12
3	Time-Series of Meteosat-10 and -12 infrared 10.5 / 10.8 μ m channel background departure statistics and data count, averaged over all pressures and the full geostationary disc	13
4	Time-Series of Meteosat-10 and -12 water vapour 6.3 μ m channel background departure statistics and data count, averaged over all pressures and the full geostationary disc	14
5	Profiles of background departure statistics of infrared window and water vapour absorption channels, for data with QI>85 and passing a background check	15
6	Profiles of background departure statistics of visible and infrared 3.8 μ m (Meteosat-12 only) channels, for data with QI>85 and passing a background check	16
7	Background departure statistics and observation count for high level inrared window AMVs, covering the dates 20241104-20250513	17
8	Background departure statistics and observation count for high level water vapour $6.3\mu m$ AMVs, covering the dates $20241104-20250513$	17
9	Background departure statistics and observation count for high level water vapour $7.3\mu m$ AMVs, covering the dates $20241104-20250513$	18
10	Mean background departure and number of observations for infrared window channel AMVs, for data with QI>85 and passing background check	19
11	Change in standard deviation of 12 hour forecasts against conventional wind observations when assimilating Meteosat-12 AMVs hourly, or assimilating Meteosat-10 AMVs, versus no AMVs at 0° longitude position. Values of less or more than 100.0 indicate better or worse 12 hour forecast agreement with the conventional wind observations, respectively. The error bars show the statistical significance of the results at each level.	20
12	Change in standard deviation of 12 hour forecasts against surface observations when assimilating Meteosat-12 AMVs hourly, or assimilating Meteosat-10 AMVs, versus no AMVs at 0° longitude position	20
13	Changes to model wind field forecast scores for Meteosat-10 and -12 assimilation versus no 0° Meteosat, verified using the operational ECMWF analysis as truth at the forecast validity time. Scores are measured in terms of normalised differences in the root-mean-square error of the forecast fields against the ECMWF operational analysis. The cross-hatching indicates statistical significance.	21



14	Changes to model geopotential height forecast scores for Meteosat-10 and -12 assimilation versus no 0° Meteosat, verified using the operational ECMWF analysis as truth at the forecast validity time.	22
15	Vertical profiles of the number of AMVs assimilated in each experiment, as a percentage change (left) and absolute number (right).	23
16	Change in standard deviation of 12 hour forecasts against conventional wind observations when assimilating MTG AMVs hourly, and Meteosat-10 AMVs at OCA pressures, versus a reference that assimilated Meteosat-10 AMVs at CLA pressures (left) and OCA pressure (right)	24
17	Change in standard deviation of observations versus background differences for ATMS (left) and conventional winds (right)	24
18	Change in standard deviation of 12 hour forecasts against conventional wind observations when adding the 3.8 μ m channel Meteosat-12 AMVs, versus a reference that assimilated Meteosat-12 AMVs from the other available channels.	25
19	Change in standard deviation of 12 hour forecasts against surface observations when adding the 3.8 μ m channel Meteosat-12 AMVs, versus a reference that assimilated Meteosat-12 AMVs from the other available channels	25



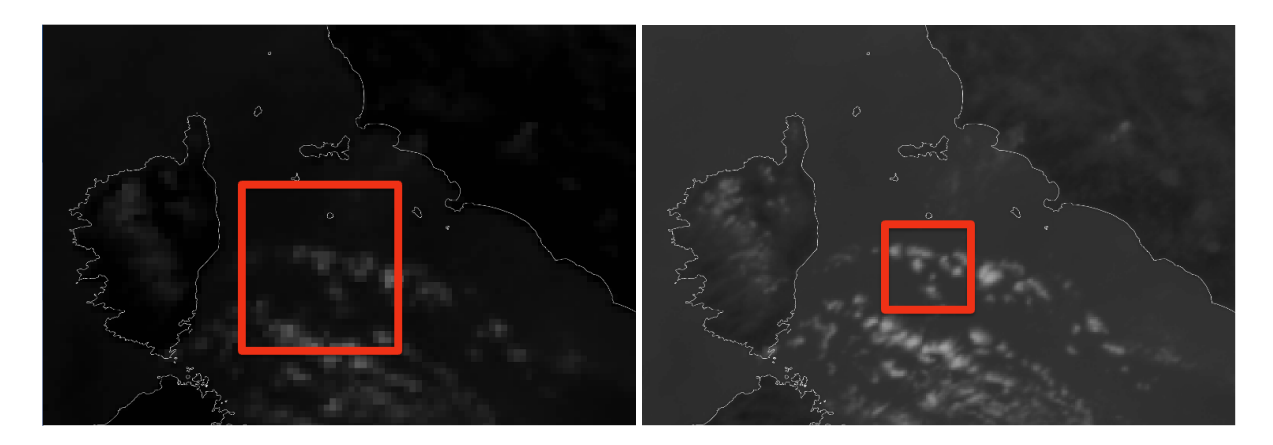


Figure 1: SEVIRI 10.8 μ m (left) and FCI 10.8 μ m (right) imagery from 3rd July 2025, 0830 UTC. Red boxes indicate the size of the AMV target.

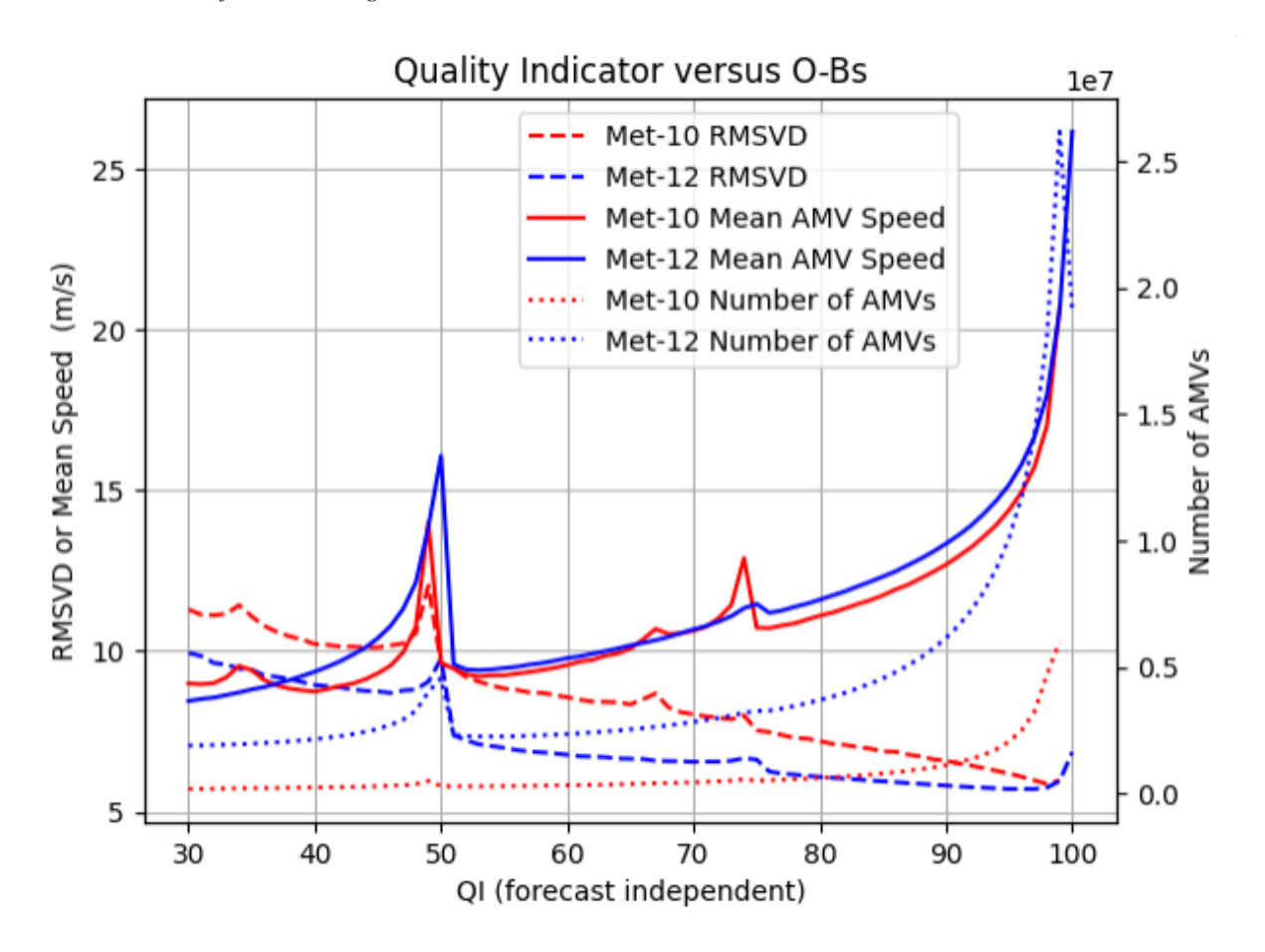


Figure 2: Variation of RMSVD against the background, mean AMV speed, and AMV count with forecast-independent quality indicator, for Meteosat-10 and -12 infrared 10.5 / 10.8 μ m channel AMVs, 20241104-20250513. Meteosat-12 AMVs with QI < 30 are available but are not shown here.



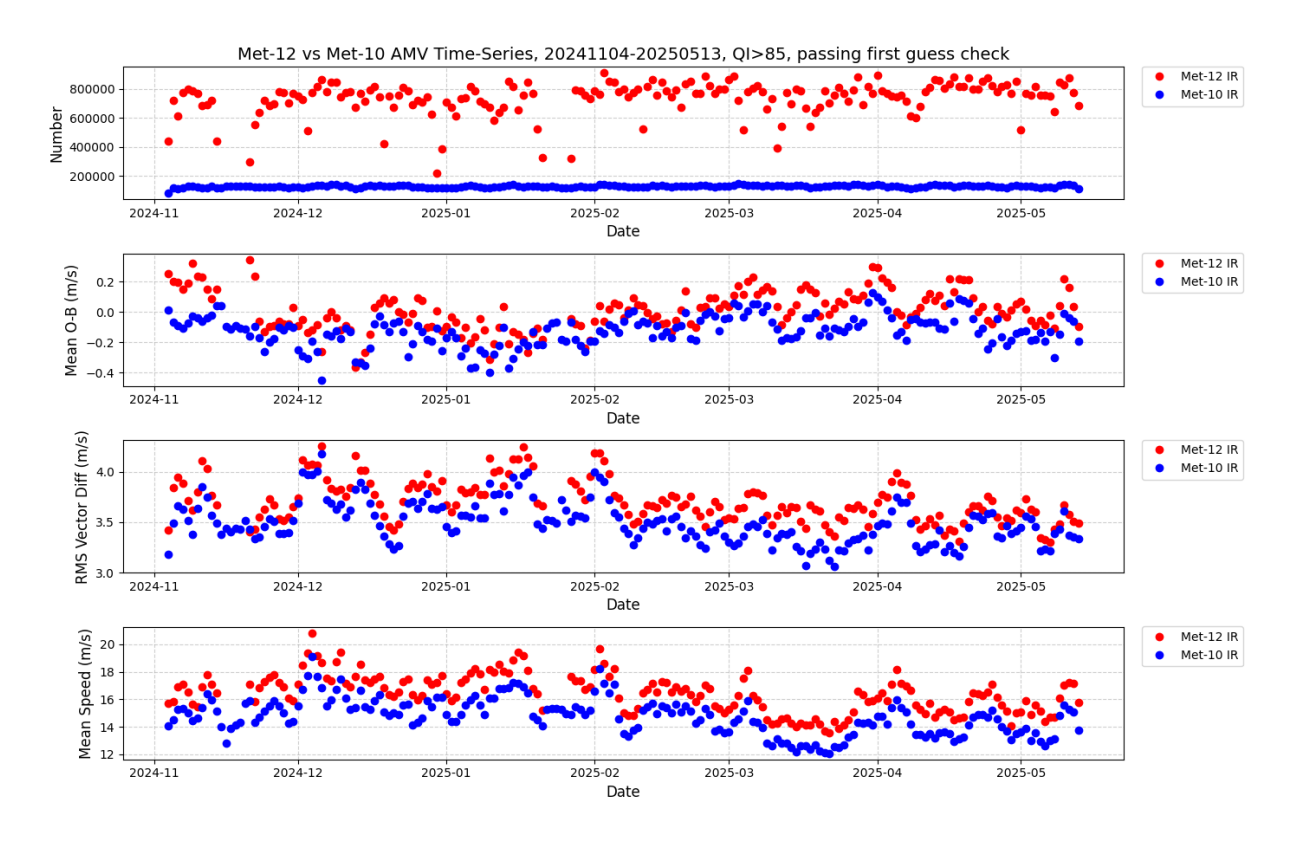


Figure 3: Time-Series of Meteosat-10 and -12 infrared $10.5 / 10.8 \mu m$ channel background departure statistics and data count, averaged over all pressures and the full geostationary disc.



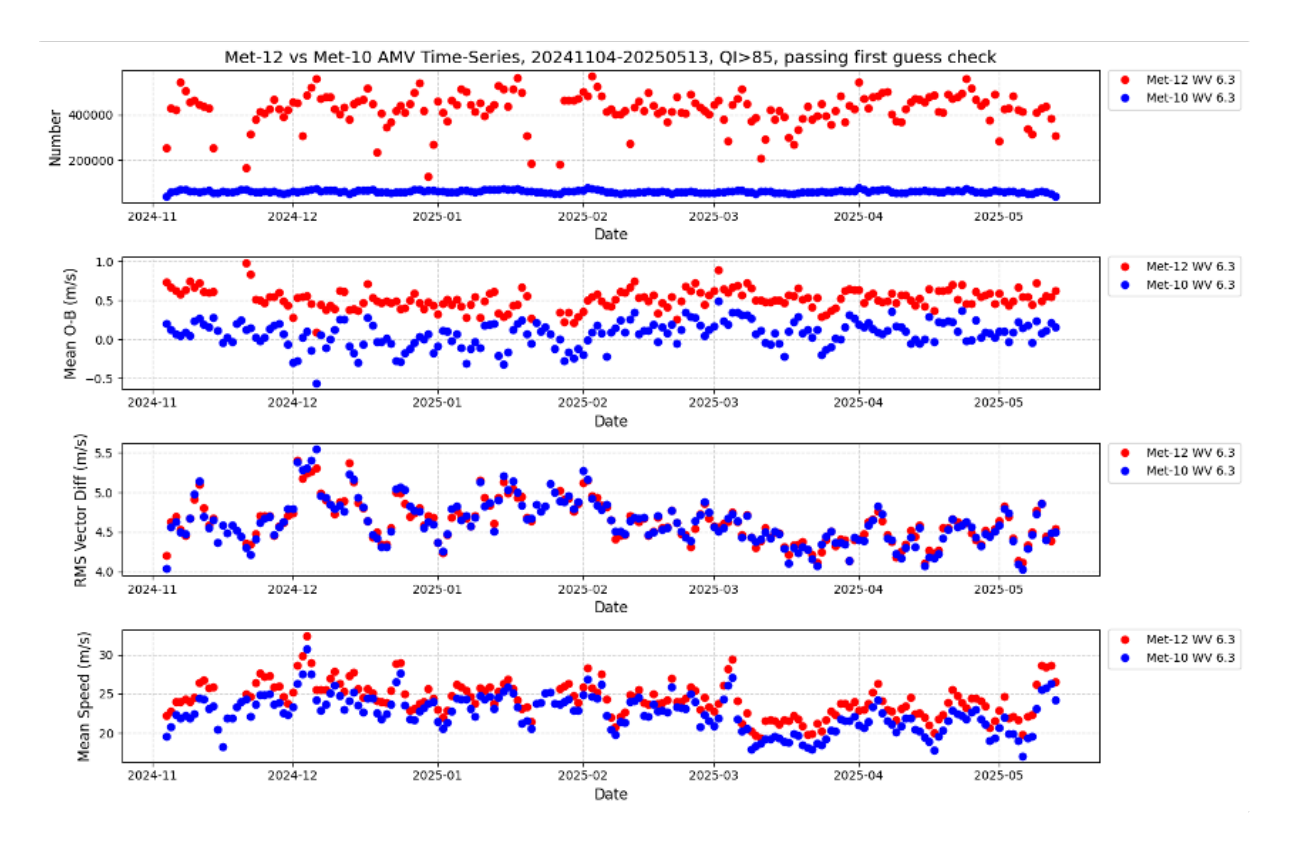


Figure 4: Time-Series of Meteosat-10 and -12 water vapour 6.3 µm channel background departure statistics and data count, averaged over all pressures and the full geostationary disc.



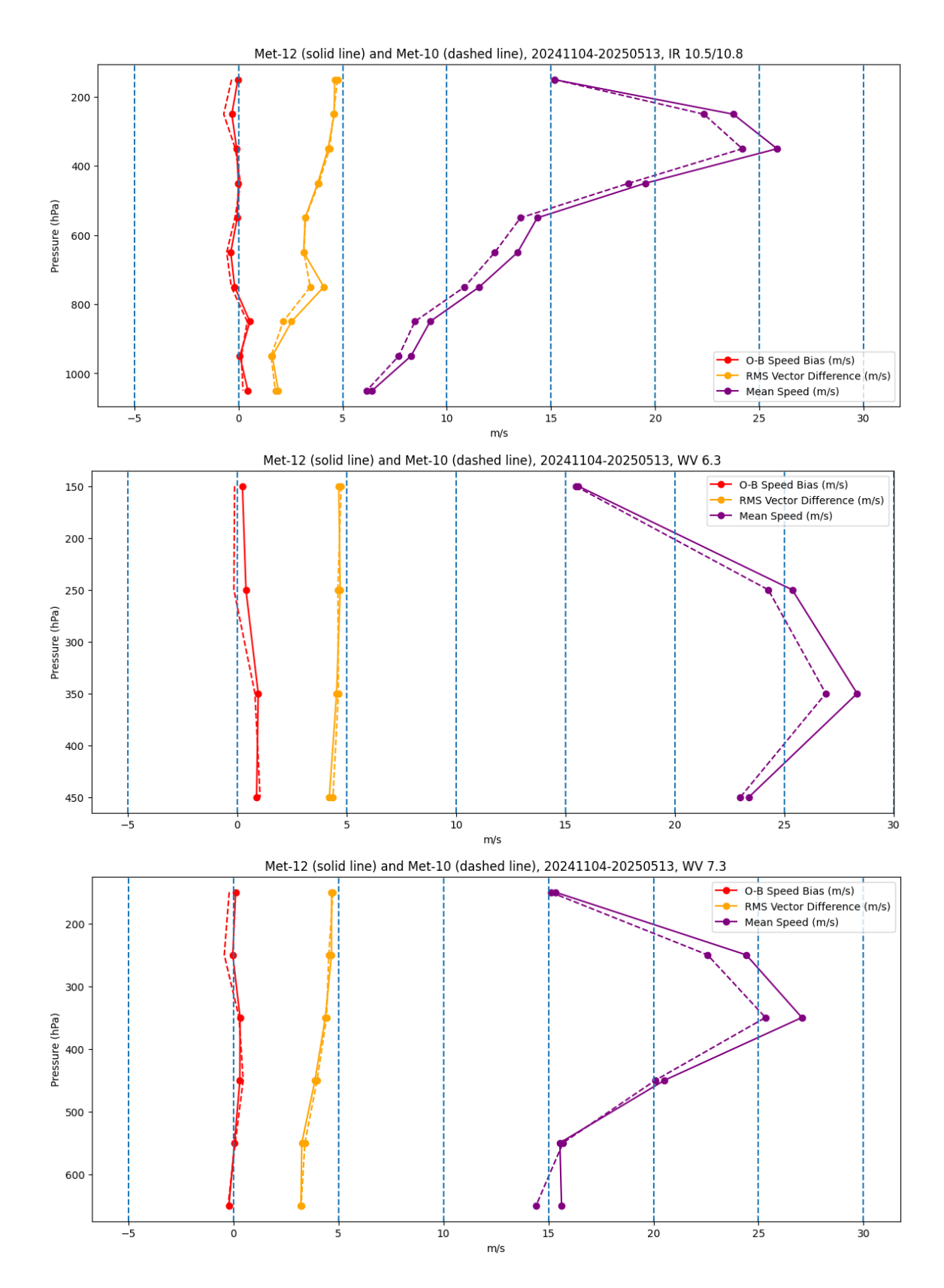


Figure 5: Profiles of background departure statistics of infrared window and water vapour absorption channels, for data with QI>85 and passing a background check.



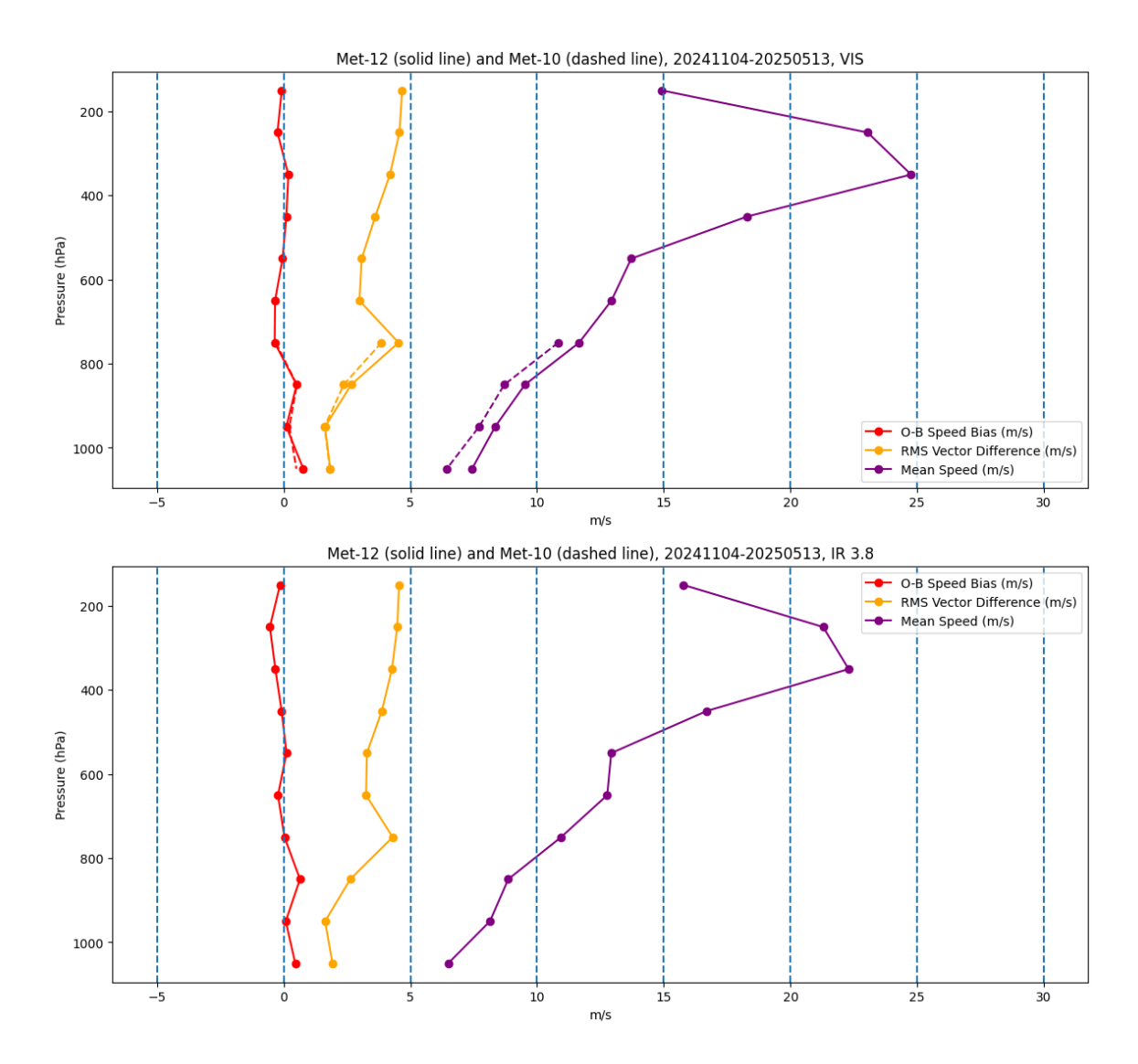


Figure 6: Profiles of background departure statistics of visible and infrared 3.8 μ m (Meteosat-12 only) channels, for data with QI>85 and passing a background check.



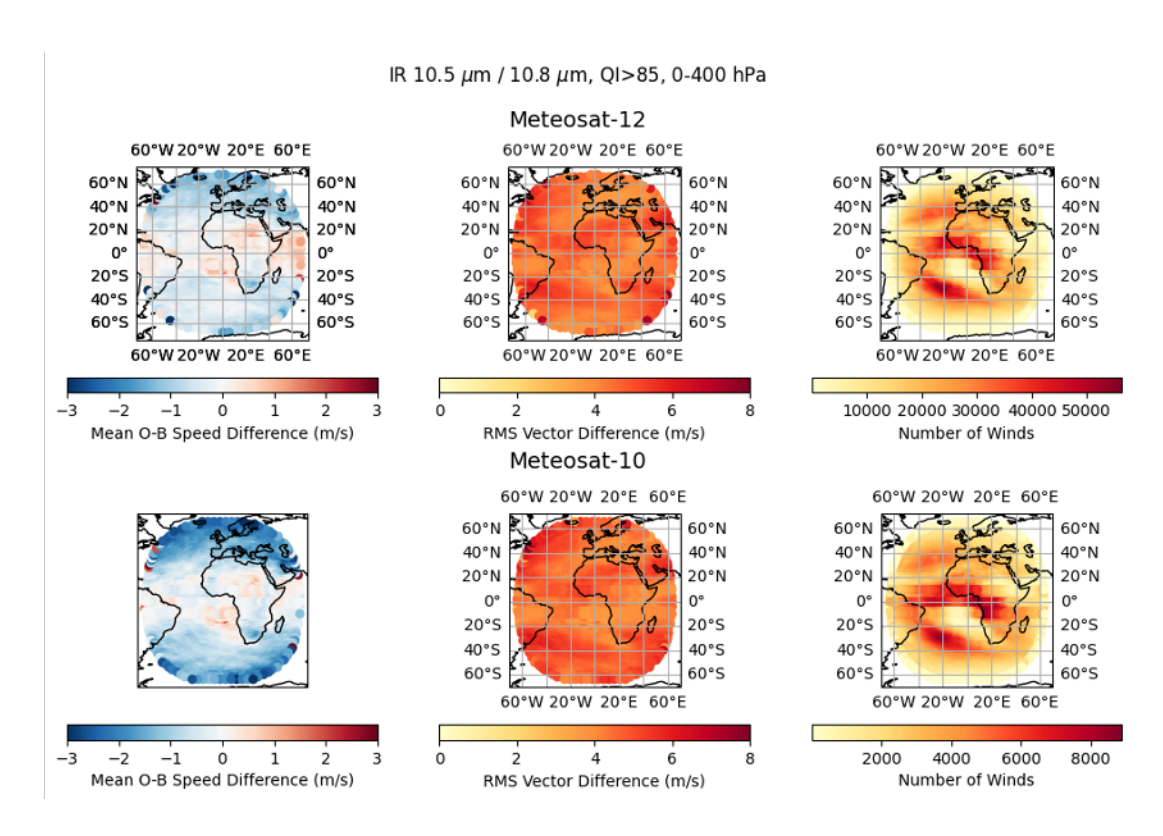


Figure 7: Background departure statistics and observation count for high level inrared window AMVs, covering the dates 20241104-20250513.

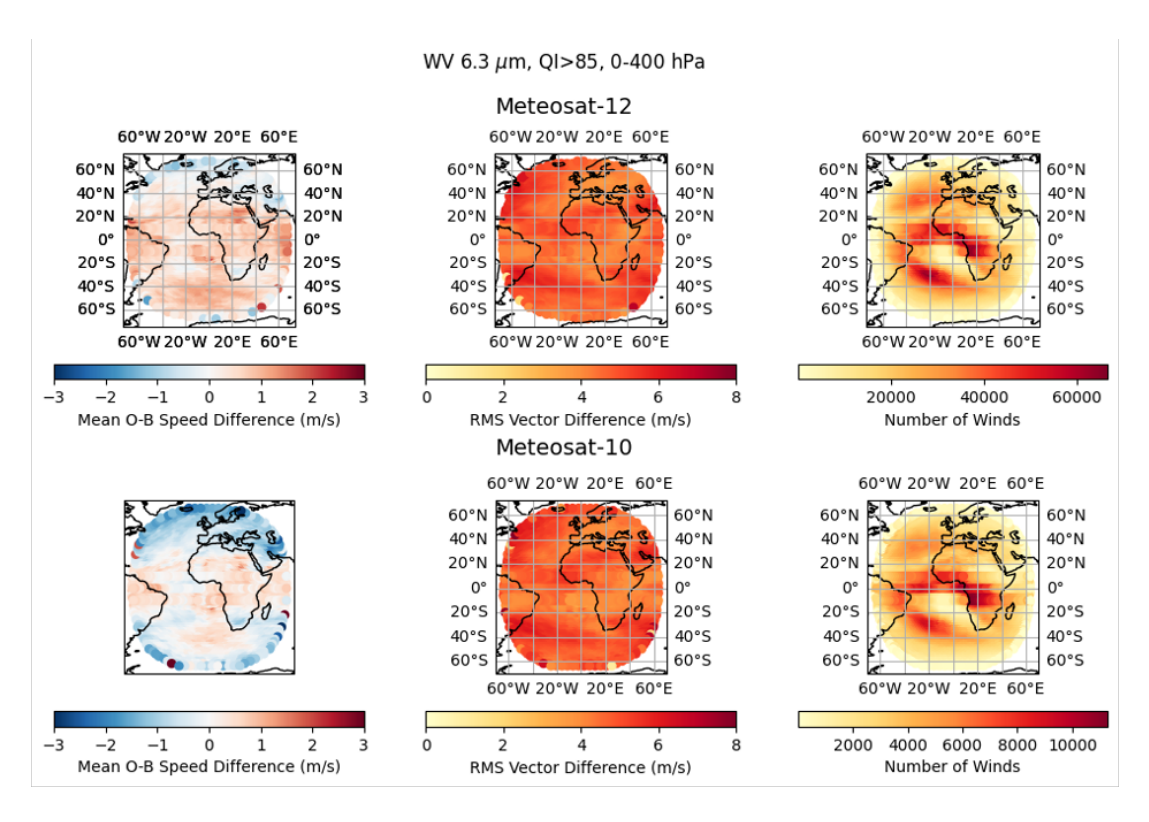


Figure 8: Background departure statistics and observation count for high level water vapour 6.3µm AMVs, covering the dates 20241104-20250513.



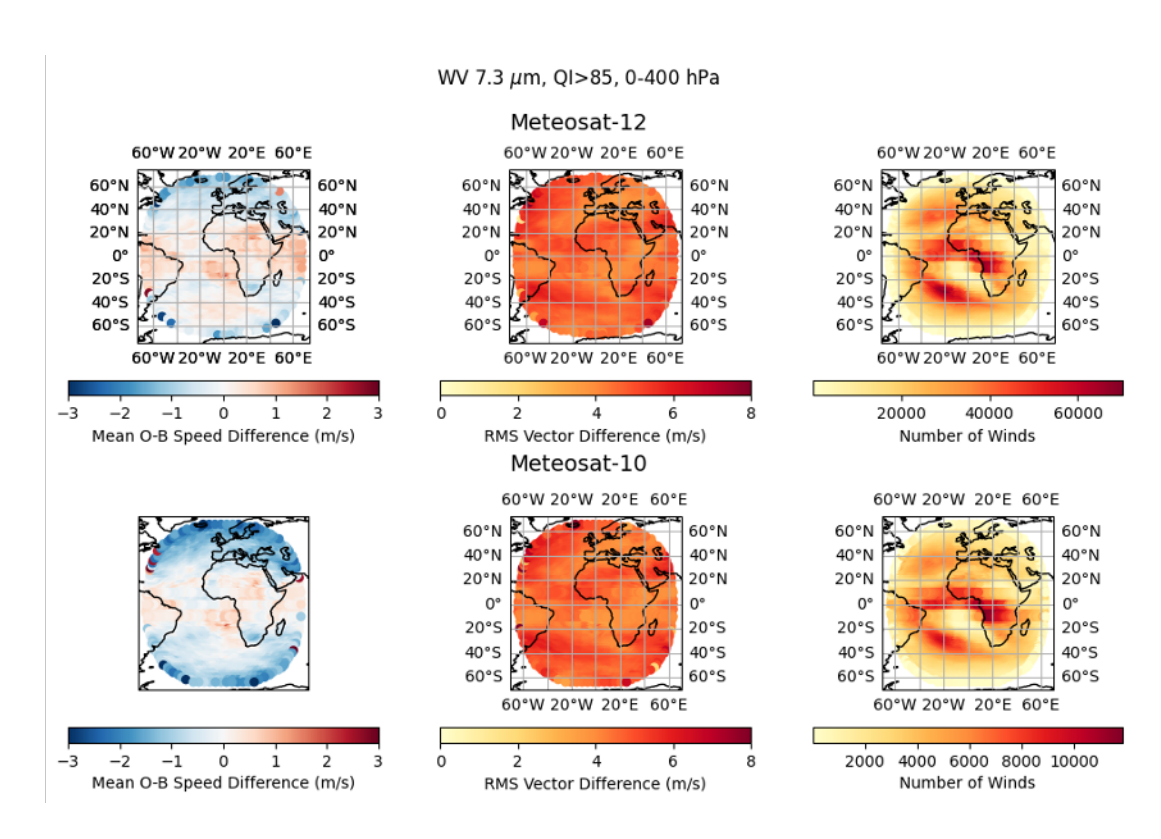


Figure 9: Background departure statistics and observation count for high level water vapour 7.3µm AMVs, covering the dates 20241104-20250513.



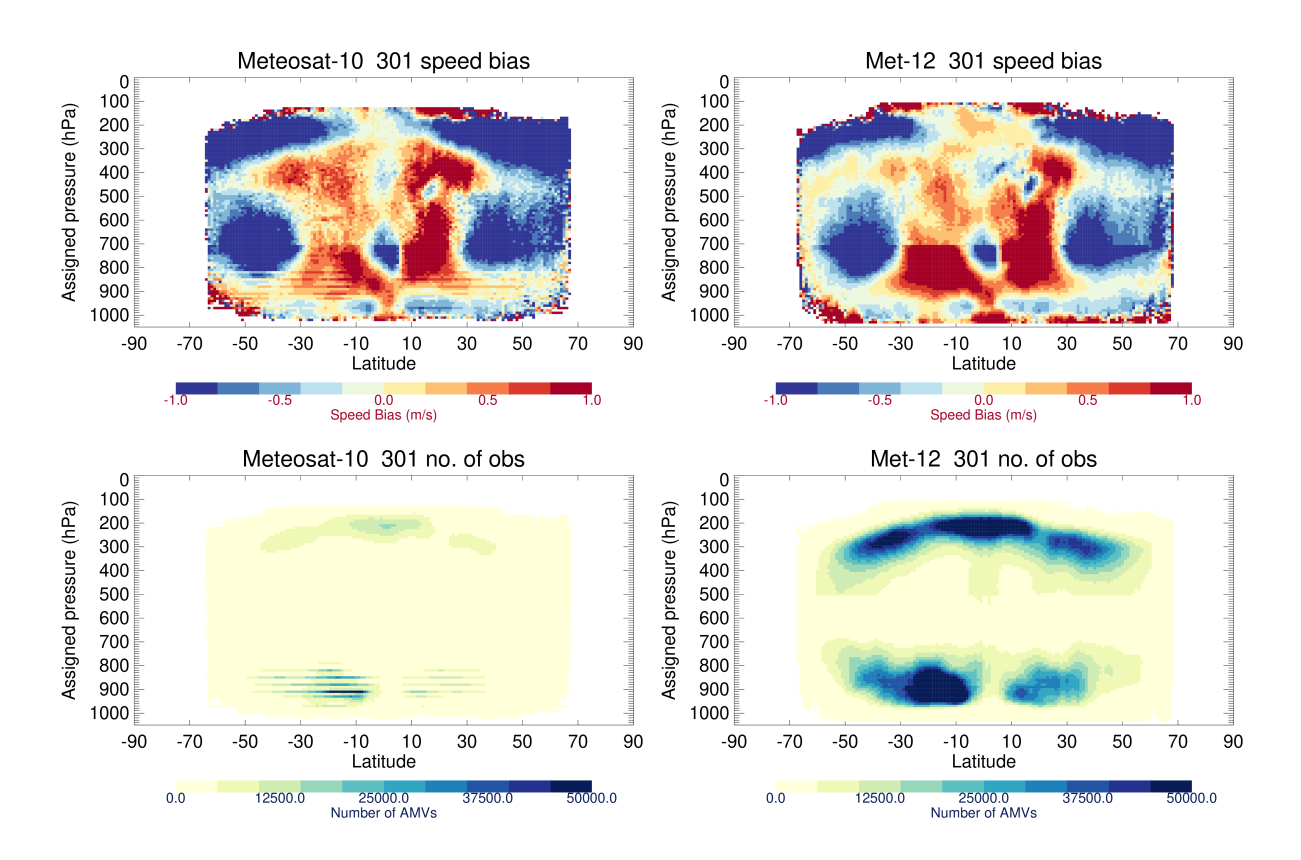
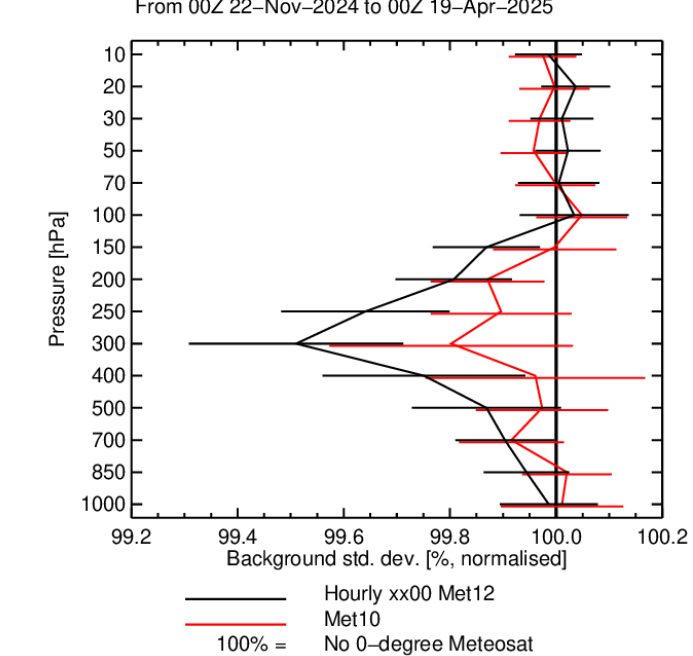


Figure 10: Mean background departure and number of observations for infrared window channel AMVs, for data with QI>85 and passing background check.





Instrument(s): AMDAR DROP MODE–S PILOT PROF TEMP – U V Area(s): met10disc From 00Z 22–Nov–2024 to 00Z 19–Apr–2025

Figure 11: Change in standard deviation of 12 hour forecasts against conventional wind observations when assimilating Meteosat-12 AMVs hourly, or assimilating Meteosat-10 AMVs, versus no AMVs at 0° longitude position. Values of less or more than 100.0 indicate better or worse 12 hour forecast agreement with the conventional wind observations, respectively. The error bars show the statistical significance of the results at each level.

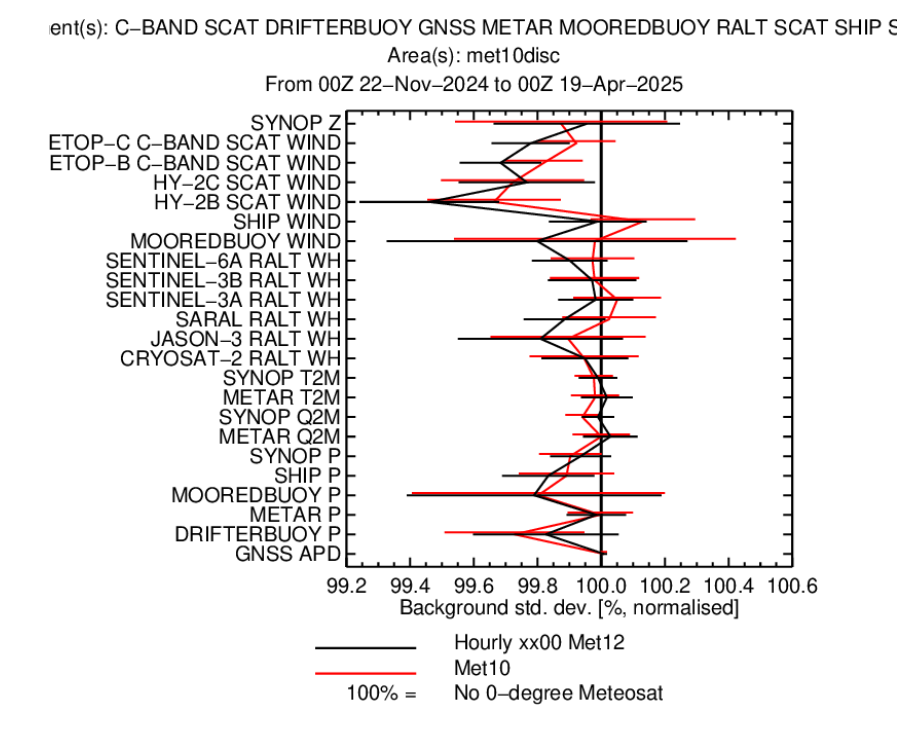


Figure 12: Change in standard deviation of 12 hour forecasts against surface observations when assimilating Meteosat-12 AMVs hourly, or assimilating Meteosat-10 AMVs, versus no AMVs at 0° longitude position.



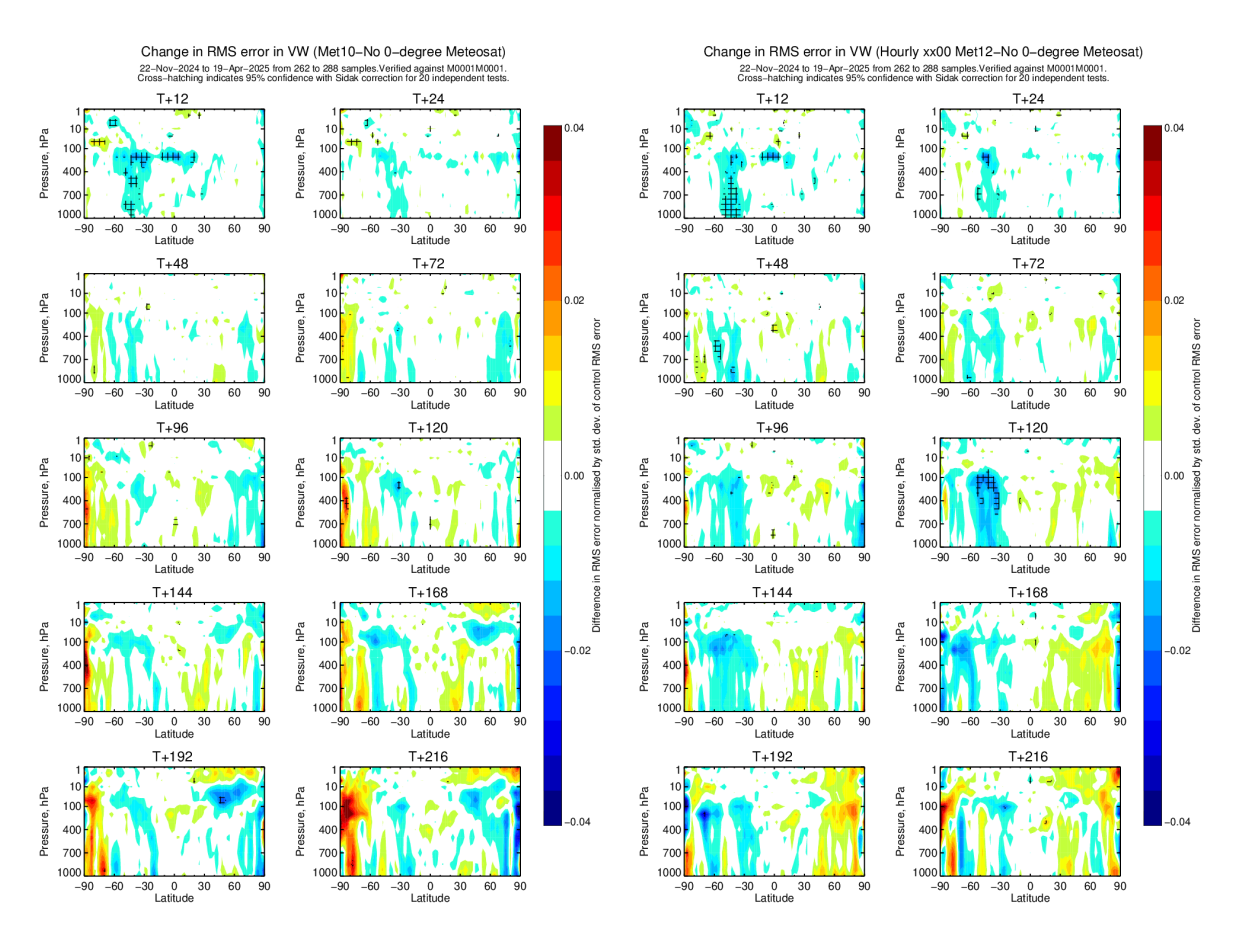


Figure 13: Changes to model wind field forecast scores for Meteosat-10 and -12 assimilation versus no 0° Meteosat, verified using the operational ECMWF analysis as truth at the forecast validity time. Scores are measured in terms of normalised differences in the root-mean-square error of the forecast fields against the ECMWF operational analysis. The cross-hatching indicates statistical significance.



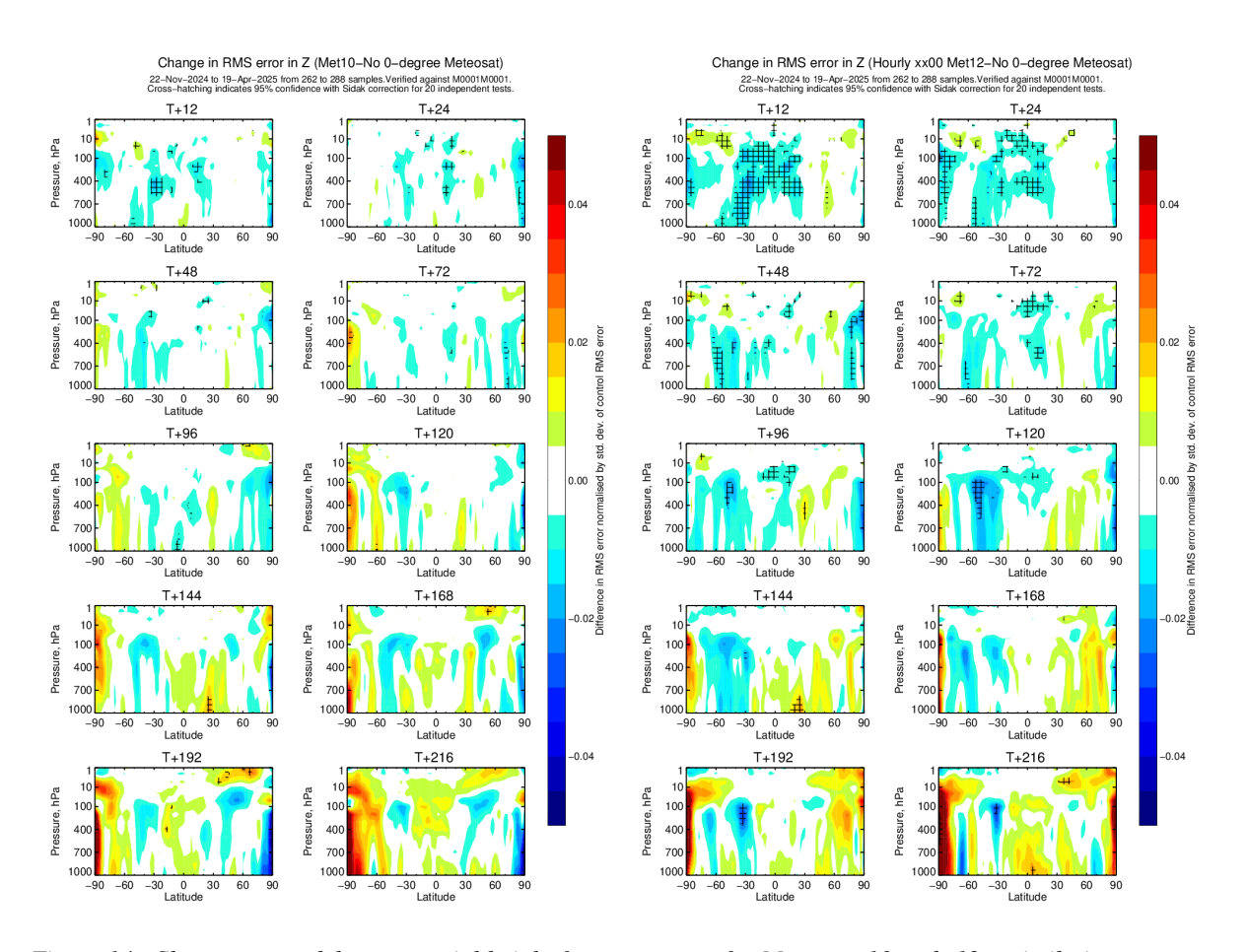


Figure 14: Changes to model geopotential height forecast scores for Meteosat-10 and -12 assimilation versus no 0° Meteosat, verified using the operational ECMWF analysis as truth at the forecast validity time.



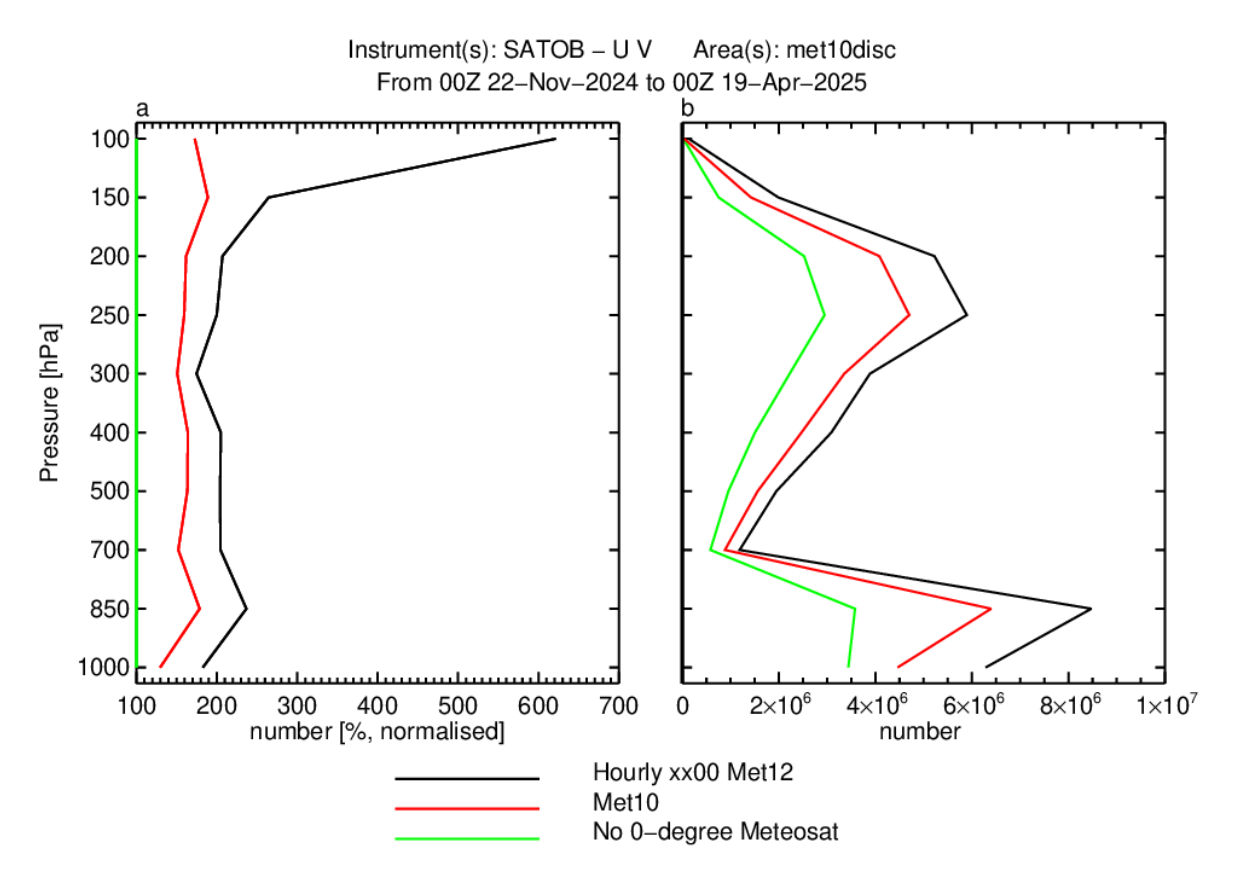


Figure 15: Vertical profiles of the number of AMVs assimilated in each experiment, as a percentage change (left) and absolute number (right).



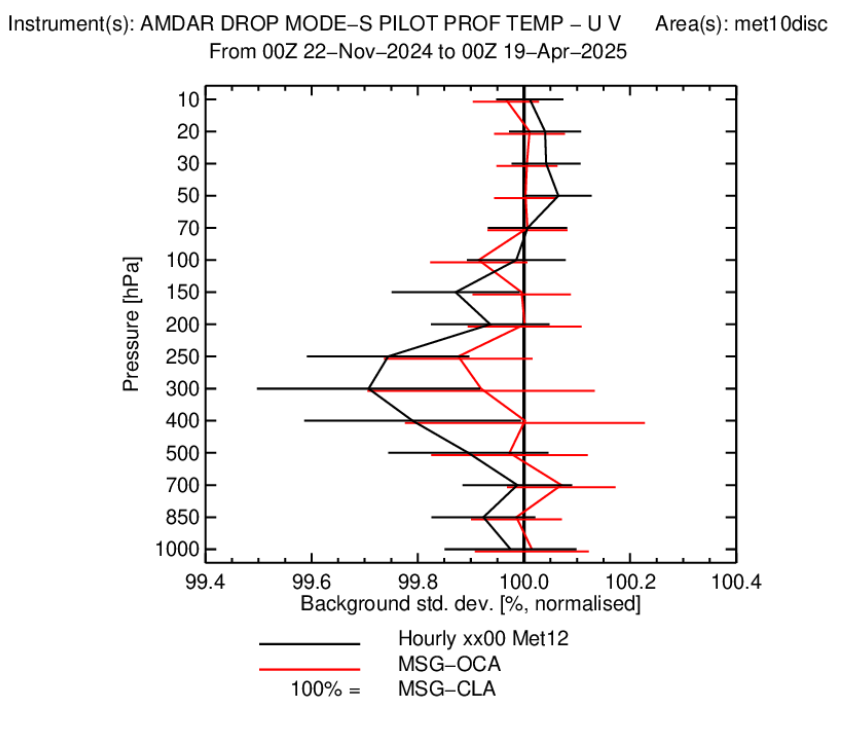


Figure 16: Change in standard deviation of 12 hour forecasts against conventional wind observations when assimilating MTG AMVs hourly, and Meteosat-10 AMVs at OCA pressures, versus a reference that assimilated Meteosat-10 AMVs at CLA pressures (left) and OCA pressure (right).

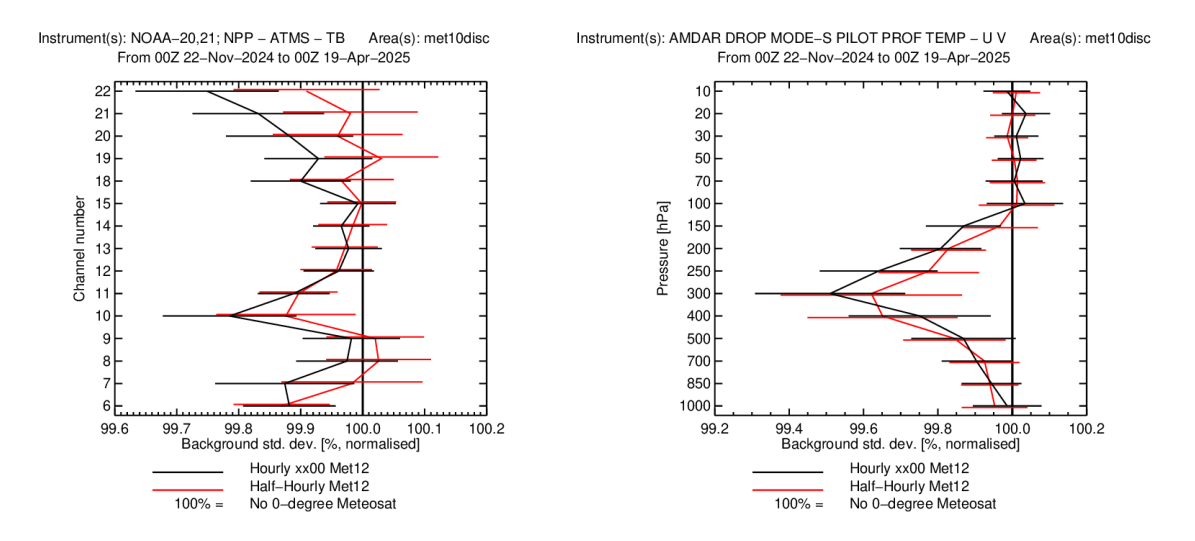
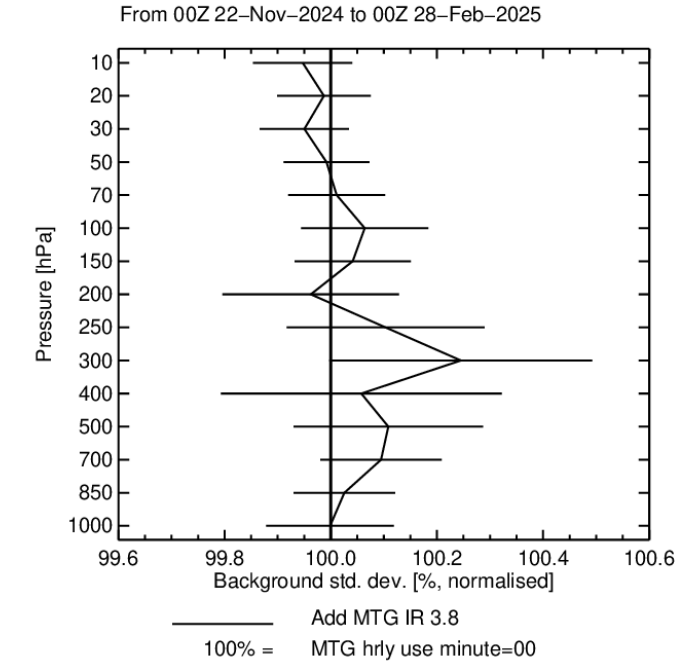


Figure 17: Change in standard deviation of observations versus background differences for ATMS (left) and conventional winds (right).





Instrument(s): AMDAR DROP MODE–S PILOT PROF TEMP – U V Area(s): met10disc From 00Z 22–Nov–2024 to 00Z 28–Feb–2025

Figure 18: Change in standard deviation of 12 hour forecasts against conventional wind observations when adding the 3.8 µm channel Meteosat-12 AMVs, versus a reference that assimilated Meteosat-12 AMVs from the other available channels.

ent(s): C-BAND SCAT DRIFTERBUOY GNSS METAR MOOREDBUOY RALT SCAT SHIP \$

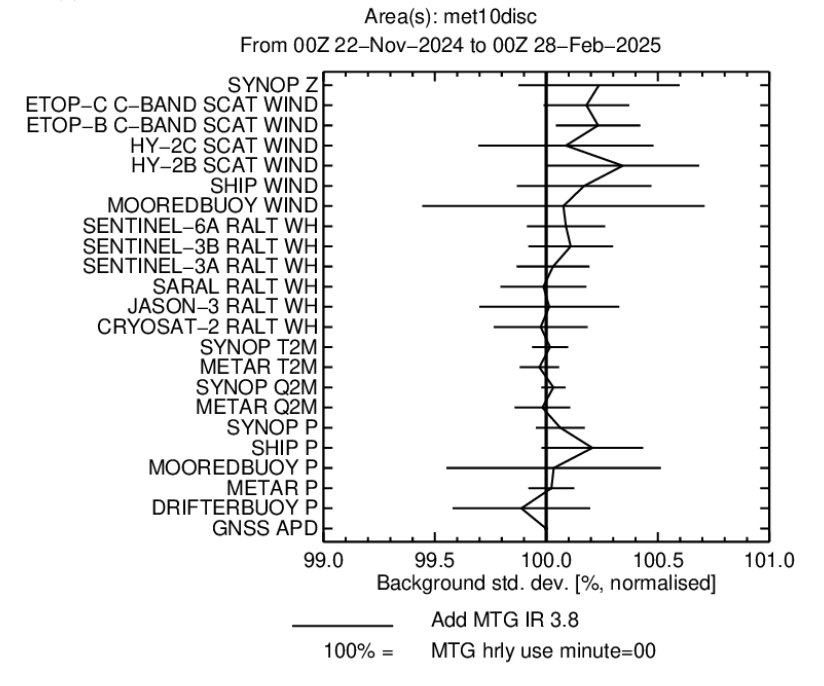


Figure 19: Change in standard deviation of 12 hour forecasts against surface observations when adding the 3.8 µm channel Meteosat-12 AMVs, versus a reference that assimilated Meteosat-12 AMVs from the other available

channels.